A Three-Dimensional Structural Dissection of *Drosophila* Polytene Chromosomes

Yoji Urata, Susan J. Parmelee, David A. Agard, and John W. Sedat

Department of Biochemistry and Biophysics and The Howard Hughes Medical Institute, University of California, San Francisco, California 94143-0554

Abstract. We have analyzed the three-dimensional structural details of *Drosophila melanogaster* polytene chromosome bands and interbands using three-dimensional light microscopy and a novel method of sample preparation that does not involve flattening or stretching the chromosomes. Bands have been visualized in unfixed chromosomes stained with the DNA specific dye 4,6-Diamidino-2-phenylindole (DAPI). Interbands have been visualized using fixed chromosomes that have been immunostained with an antibody to RNA polymerase II. Additionally, these structures have been analyzed using in situ hybridization with probes from specific genetic loci (*Notch* and *white*).

Bands are seen to be composed of ~36 substructural features that measure 0.2–0.4 μm in diameter. We suggest that these substructural features are in fact longitudinal fibers made up of bundles of chromatids. Band shape can be a reproducible characteristic of a particular band and is dependent on the spatial relationship of these bundles, varying from bands with a uniform distribution of bundles to bands with a peripheral concentration of chromatin. Interbands are composed of bundles of chromatids of a similar size and number as those seen in the bands. The distribution of bundles is similar between a band and the neighboring interband, implying that there is a long range organization to the DNA that includes both the coding and the noncoding portions of genes. Finally, we note that the polytene chromosome has a circular shape when viewed in cross section, whether there are one or two homologs present.

A fundamental unsolved problem in biology is the organization of the eukaryotic genome in the interphase nucleus. During interphase, chromatin must be maintained in structures that allow site-specific regulated transcription and temporally controlled DNA replication. Normally, it is not possible to resolve individual chromosomes in the interphase nucleus by light microscopy. However, due to the process of polytenization, the giant salivary gland chromosomes of *Drosophila melanogaster* are large enough to visualize, thus providing an excellent model system for studying interphase processes. Polytenization occurs in nearly all larval tissues and is a result of a modified cell cycle, which alternates between S phase and G phase (Smith and Orr-Weaver, 1991). The polytene nuclei in salivary gland tissue can undergo up to 10 cycles of replication without intervening divisions. The unsegregated sister chromatids and homologs remain aligned, producing banded chromosomes with a diameter of approximately three microns that are functionally in interphase. The overall architecture of the polytene chromosome must reflect the structures and interactions of chromatin at a molecular level. Thus, a study of the large-scale structure of a polytene chromosome may lead to an understanding of the fine structure details of chromatin organization. Furthermore, because the banding pattern is heritable and can be correlated with the genetic map (Bridges, 1942 and references therein), polytene chromosomes provide a unique opportunity to directly investigate the structure of interphase chromatin at specific genetic loci.

Ever since the discovery of polytene chromosomes, there has been much speculation as to the significance of the bands (Beermann, 1972; Zhimulev et al., 1981*a*; Sorsa, 1988*b*). The number of bands has been counted by light and electron microscopy. In several different regions, estimates have been made for the number of genes residing in a defined number of bands using deletion analysis and mutational saturation studies. These studies invariably find that there is an approximately equal number of genes and bands. However, some bands have been found that are multigenic and others have no discernible function (Berendes, 1970; Hochman, 1971; Lefevre, 1974; Young and Judd, 1978; Keppy and Welshons, 1980; Spierer and Spierer, 1983; Zhimulev and Belyaeva, 1991). The idea

Y. Urata and S. J. Parmelee both contributed equally to the work presented herein.

Please address all correspondence to J. W. Sedat, Department of Biochemistry and Biophysics and The Howard Hughes Medical Institute, University of California, San Francisco, CA 94143-0554. Tel.: (415) 476-4156. Fax: (415) 476-1902.

The current address of Y. Urata, Department of Pathology, Kyoto Prefectural University of Medicine, Kyoto 602, Japan.

that each band may represent a single gene is further complicated by the occurrence of overlapping reading frames (Eveleth and Marsh, 1987) and coding regions that reside in the introns of other genes (Henikoff et al., 1986; Chen et al., 1987).

Structural models of polytene chromosomes must account for the observation that at least 95% of the total genomic DNA resides in the bands (Paul and Mateyko, 1970; Beermann, 1971) and an equal level of polytenization is found in bands and interbands (Spierer and Spierer, 1984). The idea that the increased compaction of DNA in the bands is achieved by a higher order folding of parallel chromatids explains the existence of banded structures (DuPraw and Rae, 1966, Sorsa, 1988*a*). However, details of the path of chromatids through bands and interbands is still unclear. The toroidal shape of some bands (i.e., bands that show a concentration of DNA at the periphery of the chromosome arm) has been seen in light and electron microscopic studies and has led to models that suggest that the structure of the polytene chromosome is a consequence of the packing of adjacent looping individual chromatids (Mortin and Sedat, 1982; Sorsa, 1983).

The structure that the DNA adopts in bands is not a static aspect of polytene architecture. Bands can decondense to form puffs. That the transition from band to puff is a visible manifestation of genetic activity (Ashburner, 1967) has been supported by the observation that some bands can be hormonally or developmentally activated to produce or store mRNA (Berendes, 1965; Ashburner, 1972; Zhimulev and Belyaeva, 1975). In addition, specific sequences of DNA can be inserted into defined chromosomal regions, using P element transformation, to create additional bands that decondense to form interbands or puffs upon transcriptional activation (Semeshin et al., 1986, 1989). Electron microscopy of native polytene chromosomes, prepared by microdissection, has allowed the localization of ribonucleoprotein particles, thus defining transcriptional states in interbands, puffs, and diffuse bands (Hill and Watt, 1977; Hill and Whytock, 1993). Still, it is not known how a transition from band to interband or puff structure is achieved.

One approach we have taken to determining the structure of a polytene band and interband is to define their molecular limits. Alignment of the cytology and molecular structure within a specific region encompassing the *Notch* locus has allowed specific sequences to be localized to band or interband (Rykowski et al., 1988). Using high resolution DNA in situ hybridization together with computer based image collection and analysis, Rykowski et al. (1988) found that the interband (3C6-3C7) contains 5′ regulatory sequences, while the band (3C7) contains coding sequences and introns. Data was presented showing that the compaction of the DNA in this band is compatible with its folding as a 30-nm fiber. A caveat of this work is that it was done on squashed chromosomes, that is, by using a method resulting in two-dimensional specimens. Not only is structural information lost about the originally three-dimensional chromosome, but this also causes differential stretching and possibly unfolding of the interband chromatin.

To overcome the limitations of samples that have been flattened and stretched, we have developed a system for sample preparation and analysis that minimally perturbs polytene chromosomes using three-dimensional light microscopy. We have taken advantage of a technique to isolate polytene nuclei and remove their nuclear envelopes that was developed specifically for optimal structural preservation (Sedat and Manuelidis, 1977). This has been combined with a procedure to embed samples in an optically clear polyacrylamide gel matrix allowing subsequent manipulations, e.g., fixation and imaging, to be performed without loss of three-dimensional information. Finally, wide-field microscopy and a charge-coupled device (CCD) are used to acquire three-dimensional data in a digital format that allows subsequent image processing, including deconvolution, which aid in the interpretation and analysis of this information.

Wide-field three-dimensional optical microscopy (Hiraoka et al., 1991) is used in this study for a number of reasons. First, it allows large structures, such as polytene nuclei, to be studied intact, in an aqueous, well-defined ionic environment, under conditions that will, as easily, allow the use of whole organs or even living specimens. Second, specific stains and antibodies are readily available and easily visualized using fluorescence microscopy. Third, it is possible to simultaneously label several structures, allowing substructural features to be correlated with each other as well as providing internal controls.

To provide a structural baseline for future molecular work, we have set out to describe a three-dimensional overview of the structure of the polytene chromosome bands and interbands. We have looked at band-specific structures using 4,6-Diamidino-2-phenylindole (DAPI)[1] as a DNA specific stain, allowing us to verify the integrity of morphological features at all stages of isolation, embedding and fixation procedures. We have also used immunodetection as a second method to visualize structural features of chromatin. Fluorescent detection of anti-histone antibodies and anti-polymerase II antibodies allows us to view structural features of bands and interbands, respectively. While the use of DAPI and immunostaining allows us to compare all bands with all interbands, DNA in situ hybridization can provide knowledge of the molecular biology as well as the cytology of band specific and interband specific probes at a single locus. Our initial in situ hybridization work has focused on the 3C region near the tip of the X chromosome, thus continuing analysis of an area that has been extensively studied cytogenetically (see references in Sorsa, 1988*a*). We have found from initial work, as well as ongoing subsequent analysis, that high resolution optical sectioning microscopy reveals new information that is essential for a comprehensive understanding of polytene chromosome structures. We present here, for the first time, a three-dimensional view of the structure of individual bands at high resolution in an unperturbed state.

Materials and Methods

DNA Probes

The *Notch* clones, a gift of Simon Kidd (Rockefeller University, NY),

1. *Abbreviations used in this paper*: CCD, charge-coupled device; DAPI, 4,6-Diamidino-2-phenylindole.

are fragments from a chromosomal walk spanning 120 kb (Kidd et al., 1983), cloned into the plasmids pAT 153 or pEMBL 19. The kilobase values defining the dimensions of the mixtures of probes reflect the molecular coordinate scale of S. Kidd. Three different mixes of *Notch* probes were used and are outlined in Fig. 1. The N_t probe spans 105 kb; the entire *Notch* coding region, and ~30 kb on either side of the gene. It is a mixture of 14 noncontiguous clones covering from −63.5 kb to +41.5 kb; a total of 97 kb is represented in this mix. The N_b probe includes the bulk of the coding region of *Notch*. The 5′ border of N_b is at −23 kb, thus it excludes the first exon and part of the first intron. The 3′ border of N_b is at +11.4 kb, and was chosen to include the most proximal clone in the Kidd walk that was defined as part of the band 3C7 by Rykowski et al. (1988) (Ch4.1 in her nomenclature). The N_b probe is a mixture of five noncontiguous clones that include 29.8 kb of DNA. The N_i probe spans the region 3′ of the *Notch* gene, +12 kb to +22.6 kb and is made up of three contiguous or overlapping clones. It was chosen to encompass the interband sequences between 3C7 and 3C9-10 as defined by Rykowski et al. (1988) (Crb2.5 through Er3.9 in her nomenclature). The w_t probe is a mixture of nine contiguous pBR322 plasmid vectors from −8.5 kb to +25 kb of the *white* locus (Levis et al., 1982) that were kindly provided by Robert Levis (Hutchinson Cancer Research Center, Seattle, WA). The w_t probe includes the entire *white* coding region, the 5′ regulatory region plus 20 kb of 5′ and 6 kb of 3′ flanking DNA.

Labeled DNA probes were prepared by random priming. Typically 35 μg of DNA was sonicated in 500 μl of water and checked for linearization on a 2% agarose/TBE gel with ethidium staining. A mixture of 1 μg of sonicated DNA and 12.5 μg of random hexamer oligodeoxyribonucleotide primer (Pharmacia pd$(N)_6$) were heated to 100°C for 5 min. The boiled DNA and primers were adjusted to a volume of 25 μl containing 100 mM Pipes (pH 7.0), 5 mM $MgCl_2$, 10 mM β-mercaptoethanol, 5 U Klenow polymerase, 30 μM each of the three unlabeled deoxynucleotides and 24 μM labeled deoxyuridine-triphosphate, either biotin-16-dUTP (ENZO, NY, NY), or digoxigenin-11-dUTP (Boehringer-Mannheim Biochemicals, Indianapolis, IN). Digoxigenin labeling required the presence of dTTP with an optimal molar ratio of 1:2 unlabeled:labeled deoxynucleotides. More recent experiments have used biotin-11-dCTP (ENZO, NY, NY) for increased incorporation of the biotin-labeled deoxynucleotide. DNA probes were also directly fluorescently labeled. In this case random priming was done using either fluorescein-dUTP or tetramethylrhodamine-dUTP (gifts of Dr. Dan Chelsky then at Dupont-Merck Corp., Wilmington, DE). After an overnight incubation (16°C), the labeled DNA was reduced in size to 100–300 bp by restriction enzyme digestion using a mixture of AluI, HaeIII, MspI, RsaI, and Sau3AI. Label incorporation was monitored by dot blot assay and probe size was estimated by Southern blot hybridizations.

Isolation of Nuclei

Salivary glands were dissected from well fed, climbing third instar *Drosophila melanogaster* Oregon R larvae. Nuclei were isolated according to the procedure of Sedat and Manuelidis (1977). This procedure uses buffer A (15 mM Pipes, pH 6.8, 20 mM NaCl, 60 mM KCl, 0.5 mM EGTA, 2 mM EDTA, 0.5 mM spermidine, 0.2 mM spermine, 1 mM DTT) to preserve chromosome structure (Burgoyne et al., 1970; Sedat and Manuelidis, 1977; Belmont et al., 1989). 100–200 salivary glands were hand-dissected into buffer A on ice. Glands were broken by Vortex mixing for 1 min in 100 μl of 0.1% digitonin (Calbiochem Corp., La Jolla, CA) in buffer A. After centrifugation for 10 s at the lowest possible setting in a tabletop centrifuge (~20 *g*), the nuclei in suspension were removed and stored on ice. The pellet, containing the remaining glands, was resuspended in buffer A with 0.1% digitonin. Vortexting and centrifuging were repeated until no visible pellet remained. The pooled supernatants were centrifuged for 5 min at ~ 100 *g* to sediment the nuclei. The pellet was resuspended in 100 μl of 0.1% digitonin in buffer A, followed by the addition of 100 μl 0.5% Brij 58 (Pierce Chemical Co., Rockford, IL) in buffer A. After 5 min incubation the nuclei were sedimented, washed once in buffer A, and resuspended in 50 μl of buffer A.

Removal of Nuclear Envelope and Embedding Nuclei in Polyacrylamide Gel

The polytene chromosomes were immobilized in a gel to preserve their three-dimensional structures. Our main criteria for choosing an embedding media was optical clarity. By polymerizing blocks of various agaroses and acrylamide mixtures in disposable cuvettes, we were able to scan gels in a spectrophotometer over a wavelength range of 370–630 nm and have found conditions where the absorbance varies by no more than 0.004 OD U from zero. To minimize the autofluorescence of the acrylamide, polymerization of the gel was catalyzed by sodium sulfite (Grant et al., 1973). We chose a final concentration of acrylamide to be 5% (that is 29:1 acrylamide/N,N′′- methylenebisacrylamide). The permeability of acrylamide to DNA probes was verified as follows. A sample 50 μl block of acrylamide was taken through the denaturation and renaturation steps in our in situ hybridization procedures in the presence of 0.5 mg/ml sonicated calf thymus DNA in our hybridization buffer. The block was rinsed and inserted in the well of a 2% agarose gel and electrophoresed. Although DNA fragments larger than 500 bp had been excluded from the block, no such exclusion was seen in the range of 300 bp or less, i.e., the size range we use for our in situ hybridization probes (data not shown).

Fig. 2 shows an outline of the methods for isolation of nuclei, removal of nuclear envelope, and embedding nuclei in the polyacrylamide gel. Acid-cleaned coverslips (22 × 50 mm, No. 1 1/2, Clay-Adams, Franklin Lakes, NJ) with rings of nail polish (~100 μm thick when dry, and 15 mm in diameter) were prepared. A 10-μl vol of nuclear suspension was dropped inside the ring, and then 10 μl of 4 M urea (Ultra-pure grade, ICN Biomedical, Inc., Cleveland, OH) in buffer A was added and the two were mixed by tilting. Removal of the nuclear envelope was monitored by phase contrast microscopy. When approximately half of the nuclei began to open, 20 μl of a 10% acrylamide mixture (that is 10% 29:1 acrylamide/N,N′-methylenebisacrylamide, 15 mM ammonium persulfate, 15 mM sodium sulfite, 1 mM DTT, 1X buffer A) was added. The sample was quickly mixed by tilting and covered by a silanized coverslip (Surfasil, Pierce Chemical Co.). While optimizing this procedure, it was noted that there is an inverse correlation between the ease with which the nuclear envelope can be removed and the final morphology of the chromosome bands. As increases are made in either the pH of the buffer A (from pH 6.0 to 7.4), or the urea concentration (final concentration up to 4 M), the envelopes are more readily dissolved off the nuclei. However, at this higher pH or higher urea concentration, the nuclei are more likely to show a larger number of distorted structures, that is, the chromosomes may be flattened or torn looking or lose their distinct banding pattern (data not shown).

After 30 min at room temperature for polymerization, the coverslip was popped off. For immunofluorescence and in situ hybridization experiments, embedded chromosomes were fixed with 0.5 ml of 4% formaldehyde (freshly prepared from paraformaldehyde) in buffer A for 30 min at room temperature. Formaldehyde and buffer A were mixed just before use to prevent polyamine cross-linking by the formaldehyde. Otherwise, nuclei in the polyacrylamide pads were washed 3 × 5 min with buffer A, and stained with 1 μg/ml DAPI (Sigma Chem. Co., St. Louis, MO) in buffer A plus 15 mM β-mercaptoethanol for 1 h. Whole salivary glands and isolated nuclei were also embedded in the polyacrylamide gel and DAPI stained (omitting the urea treatment) without fixation as controls to estimate artificial distortion of the chromosome structure during the experimental procedures.

Immunofluorescence

Fixed nuclei were washed 3× (10 min each) in buffer A with 0.05% Tween 20 (Pierce Chemical Co.), and blocked in buffer A with 3% BSA and 0.05% Tween 20 for 30 min at room temperature. Primary antibodies were used at the following dilutions at least for 6 h in a volume of 100 μl at room temperature in a humidified chamber: 1:500 for anti-histone mAb (Chemicon, Inc., Temecula, CA); 1:100 for anti RNA polymerase II mAb (kindly provided by H. Saumweber, Max Planck Institute, Germany). Samples were washed 5× (5 min each) with buffer A, and then incubated with 100 μl of a 1:200 dilution of Texas red–labeled anti–mouse IgG, $F(ab')_2$ (Jackson Immunoresearch Labs. Inc., West Grove, PA) for 6 h at room temperature in a humid chamber. A final wash with buffer was done 5× (5 min each) to remove excessive dye and detergent traces. 6 h of incubation time was required for antibodies to penetrate deep inside chromosomes (data not shown). Controls performed only with secondary antibody resulted in negligible signals. Chromosomes were counterstained with 0.1 μg/ml for DAPI for 10 min.

DNA In Situ Hybridization and Detection of Probes

Fixed nuclei were washed 2× (10 min each) in 4ST buffer (4× SSC, 0.1% Tween-20), and then 10 min each in 20% (freshly deionized) formamide in 4ST buffer and 50% formamide in 4ST buffer. For the denaturation step, 25 μl containing 100 ng of denatured DNA probe in 50% forma-

mide/4ST buffer was layered over the sample, covered with a clean coverslip, and sealed with rubber cement. In some experiments better signal to noise ratios were achieved by using 200 ng of probe, 50 μg of competitor DNA (e.g., calf thymus DNA) and 10% dextran sulfate. The sample was denatured by heating slowly (60 min) to 70°C on a slide warmer, followed by 10 min at 70°C. Hybridization was carried out by incubation at 37°C overnight. Coverslips were removed and unhybridized probe was removed by washing (20 min each) with decreasing concentrations of formamide at room temperature. Washes were in 50, 40, 20, and 10% formamide in 4ST buffer. Two final washes (10 min each) were done using 4ST buffer.

Nonspecific binding of fluorescent labels was reduced by blocking with 100 μl of 3% BSA in 4ST buffer for 30 min at room temperature. Samples were then incubated with 100 μl of fluorescein streptavidin (Molecular Probes, Eugene, OR, 0.2 μg/ml), and/or rhodamine-sheep-anti–digoxigenin (Boehringer-Mannheim Biochemicals, 0.04 μg/ml) in 1% BSA in 4ST buffer for 1 h at room temperature. Unbound label was removed by three washes over 30 min 4ST buffer. These steps were omitted when directly fluorescently labeled probes were used. Detergent traces were removed by washing two times, for 10 min each, with buffer A. Chromosomes were counterstained with DAPI (Sigma Chemical Co.), 0.1 μg/ml, for 10 min.

Three-Dimensional Data Collection

Acrylamide films were stepped from buffer A into mounting media (80% glycerol, 2% *n*-propyl gallate, 0.25% 1,4-diazobicyclo-[2,2,2]-octaine [DABCO], pH 7.4) (Giloh and Sedat, 1982; Johnson et al., 1982) at room temperature in 20% glycerol increments for 15 min each step. Fluorescent image data were recorded using a Peltier-cooled CCD camera (Photometrics Ltd., Tucson, AZ) with 1,340 × 1,037 pixel CCD chip (Kodak-Videk) mounted on an inverted microscope IMT-2 (Olympus Corp., NY); the excitation shutter, focus movement, CCD data collection, and filter combinations were controlled by a Micro VAX III workstation (Hiraoka et al., 1990, 1991). Images were captured with a 60×, NA/1.4 oil immersion lens (Olympus Corp., NY), with an additional magnification of 1.5× or with a 100×, NA/1.4 oil immersion lens (Nikon Inc., NY), whose effective pixel sizes were 0.074 μm × 0.074 μm and 0.068 μm × 0.068 μm, respectively. To minimize spherical aberration, which is a problem when imaging samples such as ours that extend above the plane of the coverslip, data was collected using an immersion oil with a refractive index of 1.5300 (R. P. Cargille Laboratories, Inc., Cedar Grove, NJ). This oil was chosen empirically to match the index of refraction of the acrylamide block. Optical sections were recorded at 0.2-μm intervals. Multi-wavelength data were collected using a triple dichroic mirror designed for DAPI, fluorescein, and Texas red (Omega Optical, Brattleboro, VT).

A number of factors can affect the quality of the data. The signal must be intense enough that it can withstand multiple exposures of the excitation light. Fading is especially an issue when performing in situ hybridization using smaller probes because they stain less intensely. Data has been collected using probes as small as 7 kb. Although the current protocol is highly reproducible, the signal to noise ratios can vary depending on the size of the probe used and the fluorophore imaged and are in the range of 4:1 to 75:1. These ratios are determined from the deconvolved image by comparison of an average pixel intensity for the in situ hybridization signal to an average pixel intensity in an area off the chromosome. The unlabeled chromosome sometimes exhibits an additional background, though never higher than a factor of two.

Three-Dimensional Data Processing and Analysis

The three-dimensional data were corrected for photobleaching and lamp intensity variations, both of which took place during data acquisition (Shaw et al., 1989; Kam et al., 1993). Out-of-focus information was removed by a three-dimensional iterative, deconvolution method with a nonnegativity constraint (Agard et al., 1989) using an experimentally determined optical transfer function for the objective lens (Hiraoka et al., 1990).

Three-dimensional light microscopic images were visualized using an integrated multiple-window display and modeling program specially designed for analyzing complex three-dimensional structure at an image display workstation (Chen et al., 1989). While this program accommodates various formats of data display, a particularly informative way to view three-dimensional data is as a rotation projection. This is accomplished by projecting the three-dimensional data stacks onto two-dimensional images at a variety of angles, and then viewing them as stereo pairs. This can be done interactively, allowing one to rock the images from one angle to another in a movie mode. In addition, for analyzing the fine structure of single bands and interbands, the three-dimensional images were computationally dissected isolating the structure from the whole data stack. This has been done on bands that are well separated from other bands and adjacent to large interbands. Starting with a longitudinally sectioned arm, a three-dimensional data stack is rotated until the desired band is perpendicular to the plane of view. A rectangular mask is then applied around the band for the entire data stack. By selecting only the information within the masks we can create a subvolume that is specific to a single band. Recent advances in our software allow the application of a polygonal mask that may be easily modified from one section to another within a data stack. This has allowed us to "cut out" bands that previously were considered too tightly packed or variable in shape to be accurately captured. The dissected images were then further analyzed from multiple viewing angles.

In double- or triple-labeled samples, we corrected for three-dimensional translational displacement and for wavelength-dependent magnification changes (Hiroaka et al., 1991; Swedlow, J., S. Parmelee, H. Itoi, J. Sedat, and D. Agard, manuscript in preparation). We used a DAPI excitation wavelength to take three-dimensional images of DAPI-stained chromosome at both the DAPI emission wavelength and the Texas red (or rhodamine or fluorescein) emission wavelength. Thus, these two sets of three-dimensional images contained the same structural information acquired at two different wavelengths. Use of a simplex alignment scheme provided the parameters for the translation and magnification changes (Swedlow, J., S. Parmelee, H. Itoi, J. Sedat, and D. Agard, manuscript in preparation) that were then used to properly align the two data sets.

Results

A Procedure for the Preparation of Intact Three-Dimensional Polytene Chromosomes

To study polytene chromosome bands and interbands in three-dimensions, we have developed a procedure that combines three-dimensional optical sectioning microscopy with a novel chromosome immobilization scheme which together give us experimental access to these structures.

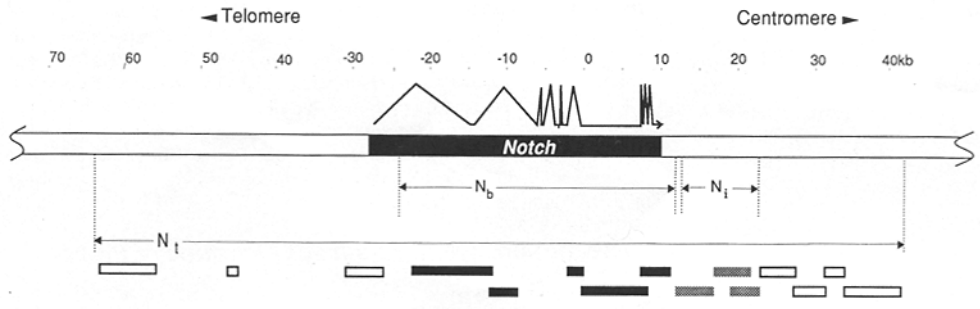

Figure 1. Molecular map of the *Notch* locus. This map is an adaptation from Rykowski et al. (1988). Orientation of the chromosome is indicated at the top. The DNA scale is marked in kb above the *Notch* transcription unit. The arrowed lines depict the distance spanned by each mix of probes. Boxes indicate the location of individual clones used to make up the mixes. Members of the mix N_b are indicated by solid boxes, members of N_i are shown as gray boxes and the mix N_t is comprised of all the clones shown (*solid*, *gray*, and *open* boxes).

Difficulties in maintaining the three-dimensionality of polytene chromosomes have been overcome by isolating nuclei from the salivary gland tissue, removing the nuclear membranes, and then embedding the resulting full set of chromosomes in an optically clear acrylamide gel for increased stability.

Fig. 2 outlines the steps for the overall procedure. This is an adaptation of a previously described method to isolate polytene nuclei which gently removes the nuclear envelope (Sedat and Manuelidis, 1977) and requires the use of a buffer specifically selected to preserve chromosome structure (Burgoyne et al., 1970). The ability of this moderate ionic strength polyamine-based buffer A to preserve chromosome structure has been documented at the resolution level of both the optical and electron microscopes (Belmont et al., 1989). Chromosome preservation has also been a major concern when choosing a method for removal of the nuclear envelope. By using a low concentration of urea in buffer A, the nuclear envelope is dissolved off but histones are not removed from the chromosomes and the polytene chromosome structure is not disrupted (Kuo et al., 1982; Mortin and Sedat, 1982).

To adapt this protocol for our use, we needed to find a method for stabilizing the chromosomes such that they retain three-dimensional structural integrity during manipulation and are easily accessible for study in the light microscope. We have sought a medium that will support the polytene chromosomes without interfering with their imaging. For this purpose, gels of polyacrylamide, that can be polymerized onto microscope coverslips, have been developed as described in Materials and Methods. These polyacrylamide gels are nonfluorescent, optically clear, durable, and compatible with both immunohistochemistry and in situ hybridization.

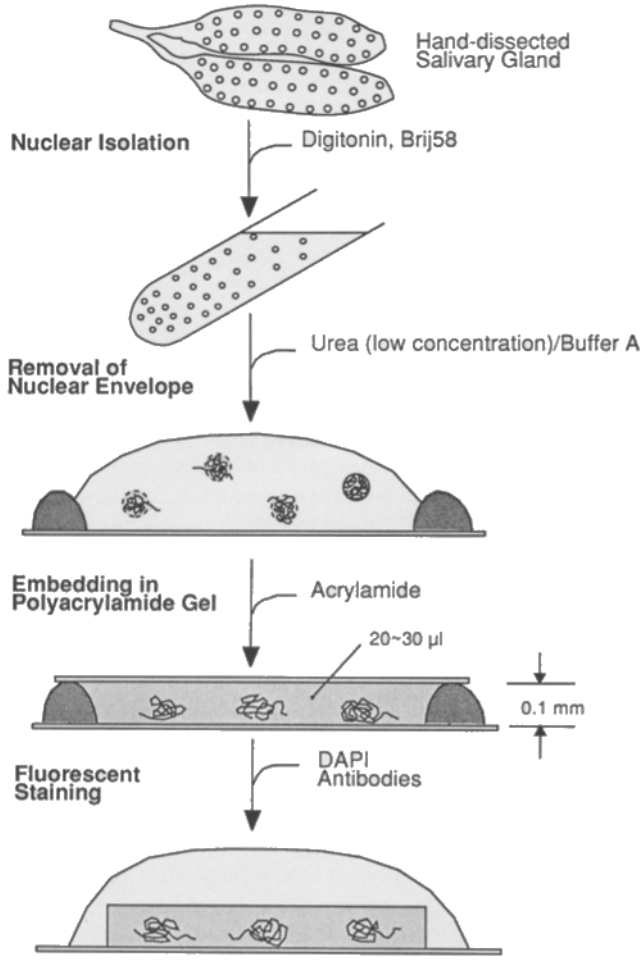

Figure 2. A schematic diagram of the procedure for preparation of three-dimensional polytene chromosome samples.

Once the polytene chromosomes have been stabilized in the polyacrylamide gel, the samples may be labeled with DAPI to specifically highlight the DNA or they can be fixed and either immunostained or in situ hybridized as described in Materials and Methods. Such fluorescently labeled samples are optically sectioned using wide-field microscopy and the resultant data stacks are deconvolved (see Materials and Methods). The final result of this procedure is a data stack of a chromosome that retains all the three-dimensional information and also has the fine structural detail to allow the cytological identification of individual bands.

The strength of this approach relies on our ability to maintain native polytene chromosome structures. To test for morphological changes that may be caused by these procedures, three-dimensional data has been taken of polytene nuclei prepared in various ways. We have embedded, in acrylamide, both whole unfixed salivary glands and isolated, unfixed nuclei with their envelopes intact. Fig. 3 shows a comparison of the results from these controls with the nuclei used for data collection: unfixed, urea-treated nuclei as well as nuclei that have been formaldehyde fixed and taken through immunostaining or in situ hybridization. Images from whole glands (Fig. 3 *a*) are adversely affected by light scattering from the secretory granules. Still, the banding pattern is distinct and variations in the concentration of DNA across the volume of the band can be seen as differences in the intensity of DAPI staining (arrows in Fig. 3). We have also found that, even after urea treatment, the bands remain phase dark under phase microscopy indicative of high refractive index features (data not shown). Furthermore, band dimensions, and band/interband spacing is preserved relative to controls. Overall, we find that the quality of the morphology seen in the controls (Fig. 3, *a* and *b*) is comparable to the morphology seen in the urea-treated nuclei (Fig. 3, *c* and *d*). In addition, we find that the structures that are stained using DAPI appear to be identical to what is seen using anti-histone antibodies (Fig. 4). Thus, these methods provide a robust system for the study and analysis of polytene interphase chromosomes structure.

A Three-Dimensional Analysis of Polytene Chromosome Bands

The careful mapping of the polytene chromosomes provides a reference for identifying individual bands (Bridges, 1942 and references therein; Lefevre, 1976; Sorsa, 1988*a*). Correspondence of our three-dimensional preparations with Bridges' revised maps is clearly evident even though conventional squashing techniques, like those used by Bridges or Lefevre, allow a greater degree of stretching. A typical example of the chromosome arm 3L is shown in

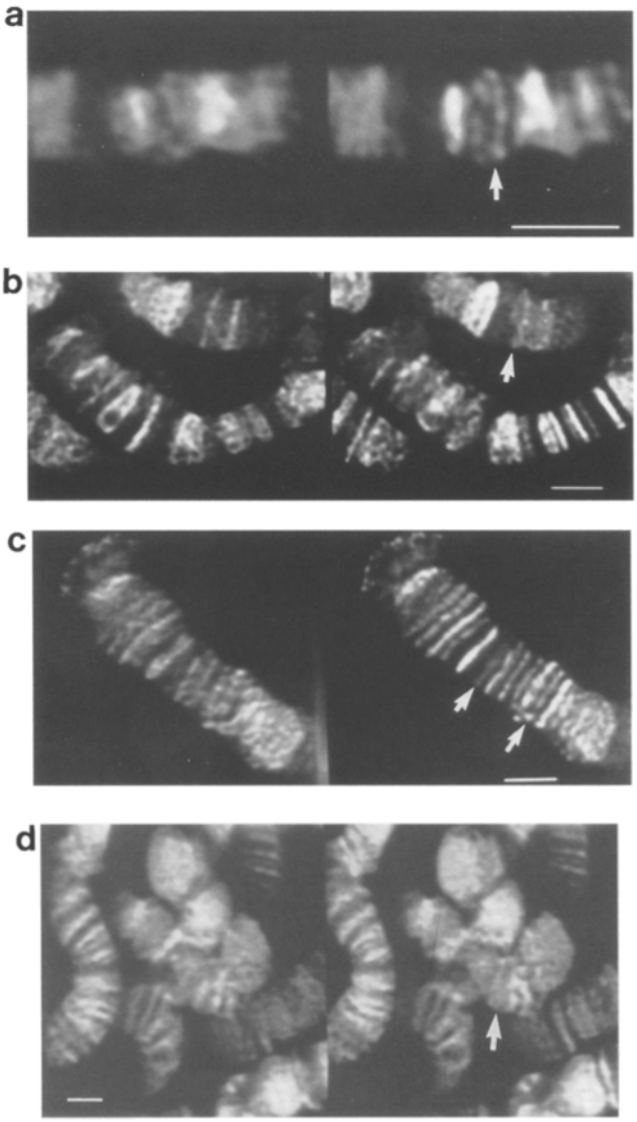

Figure 3. Preservation of chromosome morphology in nuclei with and without urea treatment. Stereo pairs are shown of polytene chromosomes taken from: a whole salivary gland (*a*), a section of 2L from an unfixed, isolated nucleus with an intact nuclear envelope (*b*), the top of 3L from an unfixed, isolated nucleus that has been treated with urea to remove the nuclear membrane (*c*), a portion of a nucleus after urea treatment, fixation and in situ hybridization (*d*) (hybridization signal not shown). Examples of bands that show peripheral concentration of DNA can be found in all samples (*arrows*). The arrows in *c* point to the bands 62A9-10 and 62D1-2 (reading from *left to right*) and are displayed in cross section in the left panel of Fig. 5 *b*. Data has been collected and processed as described in the Materials and Methods. All samples are embedded in a polyacrylamide gel layer and stained with DAPI. The scale bar represents 3 μm.

Fig. 5 *a*. It can be seen by inspection of this image that it is possible to identify not only the lettered subdivisions but also individual numbered bands within each subdivision. We can routinely identify 60% of Bridges' bands, i.e., the degree of identification expected from a photomicrograph of a squashed preparation (Sorsa, 1988*a*). The only consistent differences between Bridges' maps and our three-dimensional images is that Bridges' "doublet" bands (a Bridges' doublet represents two closely spaced similarly appearing bands) are always seen as a single band. A similar finding was noted by Berendes (1970). In summary, these preparations preserve sufficient detail to allow us to determine the three-dimensional structure of specific bands.

While three-dimensional data contains more information than two-dimensional images, there is the added complication of interpreting that data. Our lab has developed over the years a number of approaches to understanding structural information in a three-dimensional volume. One approach is to display these images as rotation projections (as described in Materials and Methods). This allows three-dimensional information to be perceived throughout the volume, often revealing structures hidden behind other features and is especially useful for complicated, densely packed objects. Fig. 3 shows four different images of polytene chromosome arms where the three-dimensional volume is displayed as stereo pairs of rotation projections. Inspection of these images reveals that a large number of bands have a distinct rim, showing less staining in the interior (*arrows*, Fig. 3). This is most noticeable in brightly staining bands or when adjacent to a large interband. Examples of polytene chromosome bands with peripheral DNA staining are seen in chromosome arms in each of fifty separate preparations including the control samples with intact nuclear envelopes (*arrows*, Fig. 3 *a*). Although we find that approximately one half of the bands viewed in rotation projections concentrate their DNA at the periphery, it is clear that this is not true for all bands.

We have found that even viewing the data as rotation projections is insufficient to allow quantification of the frequency and extent of peripheral DNA concentration in all bands. In some regions of the polytene chromosome, the bands are tightly packed and even tilting images only 5–10° interferes with the ability to fully score for the degree of peripheral DNA concentration, especially for thin bands. Thus, we have developed a method to computationally isolate single bands from a three-dimensional volume (as described in Materials and Methods). The resultant single-band subvolumes can be viewed at any tilt angle, allowing access to cross sectional views without interference of adjacent bands. Fig. 5 *b* shows the result of such a procedure. Each subvolume has been rotated from 0° to 50° tilts in 10° increments. In general we find a wide range of band architectures. Many bands have a peripheral concentration of DNA and occasionally reveal large or small "hollow" regions within the band interiors. In an attempt to quantify the frequency of these types of variations, the degree of peripheral concentration has been subjectively classified. We have distinguished between bands that show a peripheral concentration of the DNA (+), bands that have some peripheral concentration of the DNA (±), and bands that have no peripheral concentration of the DNA (−). Table I shows the results of scoring 111 bands from nine separate arms. Overall 66% of the bands were scored as showing distinct peripheral DNA concentration, 18% were scored as showing partial peripheral DNA concentration, and the remaining 16% were scored as not having any significant concentration of DNA in the periphery. Fig. 5 *b* shows examples of each band classification and illustrates a caveat of this analysis since what we find is not discrete categories but really a continuum of band shapes from two extremes.

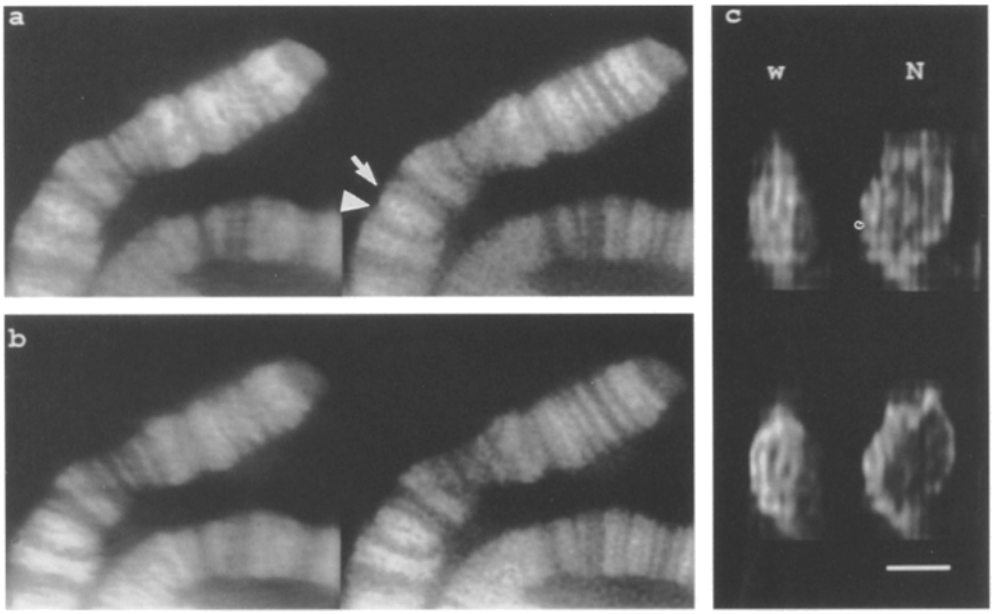

Figure 4. Comparison of the chromosomal structures labeled by DAPI staining and anti-histone antibodies: stereo pairs of chromosomes imaged at two different wavelengths shows an example of a nucleus that has been embedded in acrylamide and subsequently stained with an anti-histone mAb and DAPI. Visualization of the anti-histone staining with a Texas red–labeled secondary antibody (*a*) can be directly compared with the banding pattern produced by DAPI staining (*b*). Computational dissection of the bands 3C2 (*w*) and 3C7 (*N*) (*arrow* and *arrowhead*, respectively, in *a*) allows comparison of substructural features when viewed in cross section (*c*). (Anti-histone is shown on *top*, DAPI on *bottom*, 3C2 on the *left*, and 3C7 on the *right*). The scale bar represents 3 μm.

However, the vast majority of the bands show some peripheral concentration of DNA and an uneven distribution of DAPI staining features.

The peripheral DNA concentration of specific, cytologically identified bands has been monitored for reproducibility. Fig. 5 *b* provides several examples of computationally dissected bands from two different preparations. Examination of the same band from different nuclei suggests that there may be a common pattern of distribution of DNA at a given locus. Although this is not clear-cut for all of the bands, in some examples (for instance, bands 62A9-10, 62D1-2, and 62D5-6 in Fig. 5) that are easily categorized as having one of the extreme forms of band architecture, the DNA distribution is easily recognized as consistent between the two examples. This suggests that in some cases a specific band has a characteristic architecture based on the distribution of the DNA.

Bands have been previously categorized by Bridges as being either "singlets" or "doublets" (Bridges, 1942 and references therein; Sorsa, 1988*a*). The uncertainty of the significance of this classification, encouraged us to look for correspondence between the existence of peripheral concentration of DNA in a band and the doublet nature of those bands. Table I shows the results (see Fig. 5 for specific examples). We find that classification as a doublet is neither necessary nor sufficient to predict the distribution pattern of DNA in a band.

Although the differences between bands are clearly seen in the tilted views shown in Fig. 5, it is also obvious that there is a common punctate nature of the DAPI staining. Rather than a solid disk-like structure that one would expect if the DNA were evenly distributed, the DNA staining reveals substructural features as if the chromatids are bundled. When viewed in cross section, each band is composed of dotted or ellipsoid substructures of variable intensities sized ~0.2–0.4 μm in diameter. The number of substructural components counted in a band ranges between 25–53 (mean = 36 ± 7). This analysis includes 39 bands from five different preparations. It appears that these substructural features are in phase in adjacent bands, as if these are continuous bundles of chromatids that are joined from one band to the next. This continuity is revealed by comparing positions of substructural features in neighboring bands that have been computationally rotated to a cross sectional view, as in Fig. 5. However, since these images have been rotated, the original optical axis (Z axis) is now part of the image plane (originally the X and Y axes) and because of the decreased resolution in Z, it is often difficult to distinguish the boundaries of the substructural features. A clearer view of these structures can be seen in Fig. 6 which shows serial optical cross sections spanning 3 μm of a polytene chromosome arm. Because our preparations have been optimized to spread chromosome arms for longitudinal views, the polytene chromosome is rarely captured perpendicular to the sectioning plane of the microscope for more than a few microns of length.

Nonetheless, when these substructural features are followed from band to band for a few microns, they look like continuous fibers that merge and split as they change their position relative of each other (see Fig. 6). Unfortunately, tilting this subvolume of data 90° around the Y axis to reveal a longitudinal view, does not reveal a discrete banding pattern because of the decreased resolution in Z. However, one can estimate that three microns should span approximately five bands (compare Fig. 5 *a*).

The relationship between the two homologs in the polytene chromosome has also been investigated. Conven-

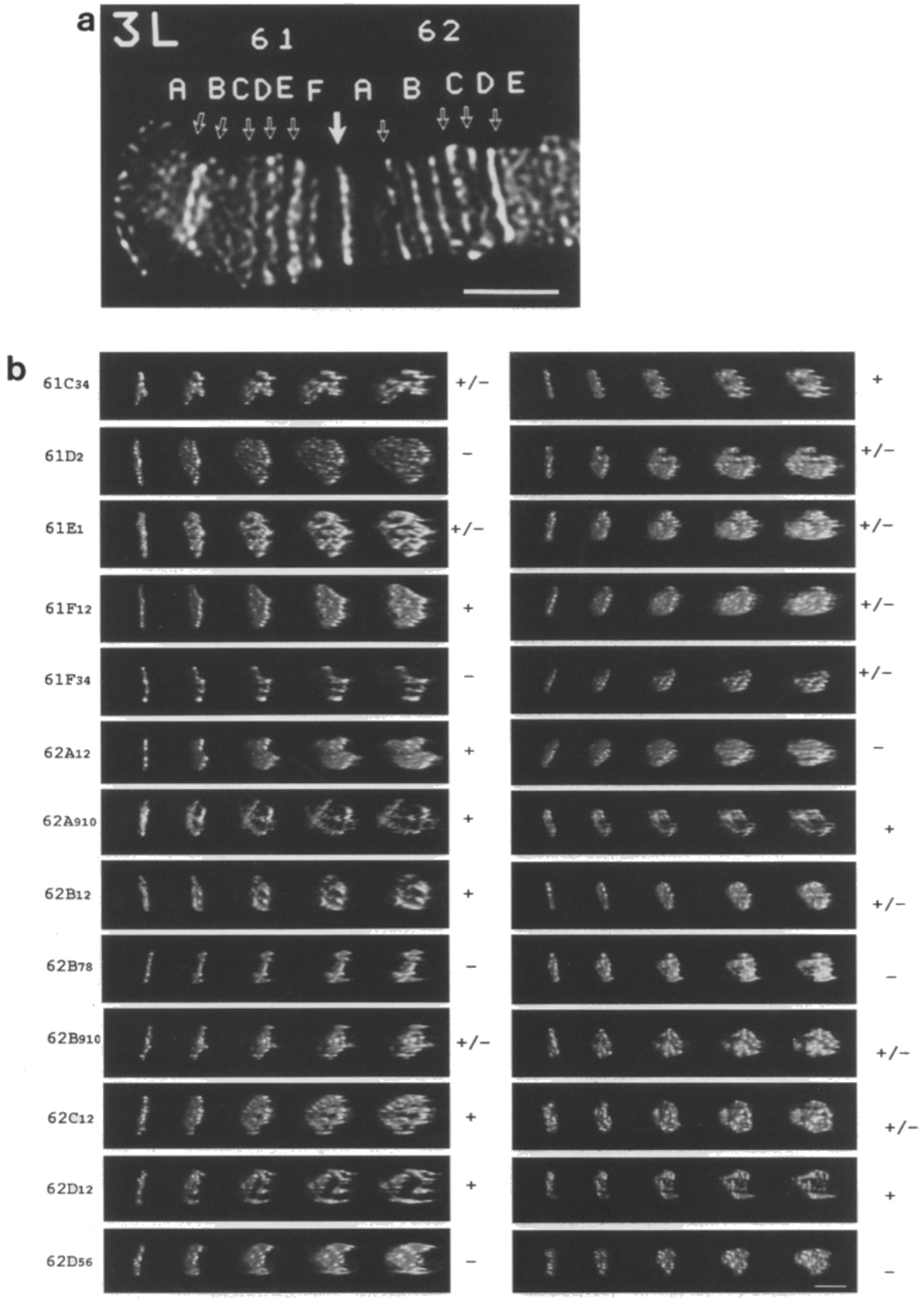

Figure 5. Three-dimensional data collection of unsquashed chromosomes yields readable cytology and allows isolation and rotation of individual bands. A single optical section from a three-dimensional data stack is shown for the tip of 3L (*a*). The cytology has been identified by comparison to the maps of Bridges and Lefevre. Numbered (*closed arrow*) and lettered (*open arrows*) regions have been la-

Table I. The Correlation of Bands with Peripheral Concentration of DNA and Their Classification as Doublets

Band type*	Peripheral concentration of DNA‡			Total
	+	±	−	
Singlets	12 (54%)	5 (23%)	5 (23%)	22
Doublets	61 (68%)	15 (17%)	13 (15%)	89
All bands	73 (66%)	20 (18%)	18 (16%)	111

*Bands have been classified as doublets or singlets as depicted in the reference maps of Bridges (Bridges, 1942 and references therein).

‡ Bands have been viewed in cross section and scored as having the majority of their DNA in the periphery (+) or having some DNA concentrated in the periphery (±) or having no peripheral concentration of DNA (−).

tional squash preparations of polytene chromosomes clearly show the two homologs separated but aligned side-by-side, and loosely coiled around one another. In unsquashed preparations polytene chromosome arms appears as a single structural unit, without any evidence of a separation between the homologs (see also Mortin and Sedat, 1982). To better understand how the homologs are organized in these polytene chromosome bands, we made use of a stock of flies that have a multiply inverted X chromosome balancer (FM7). In heterozygotes of FM7, there is a separation of each pair of homologs at the sites of inversions on the female X chromosome. We find that both paired homologs and separated homologs are cylindrical, that is, they form one or two (respectively) circles in cross section. When looking at the site of an inversion, there is no indication of random mixing of the chromatids from the two homologs, that is, the junction appears to be a clean separation. Preliminary data suggests that there may be a flattening of the cylinder that comprises the paired homologs just before the bifurcation. Both paired and unpaired homologs have the same structural features described above, although, the number of substructures counted in the separated homologs are approximately one half the number found in the aligned homolog pair.

Three-Dimensional In Situ Hybridization on Intact Polytene Chromosomes

While the study of DAPI-stained chromosomes is useful in acquiring an overview of polytene band structure, the relationship between the cytology and the DNA sequence is unknown. To allow us to look at the cytological structures of a defined sequence of DNA, we have developed a procedure for high resolution DNA in situ hybridization on these acrylamide embedded, unsquashed chromosomes. Here too, preservation of the structural integrity of the chromosomes has been an important factor in the development of this system. We have carefully monitored chromosome morphology and find that despite the relatively harsh treatment of heat and formamide required for denaturation, both general morphology and substructural features were found to be comparable in chromosomes before and after in situ hybridization. The stabilization seems to be a direct consequence of the embedment. Fig. 3 *d* shows a portion of a DAPI-stained polytene nucleus after removal of the nuclear envelope, fixation, embedding, DNA in situ hybridization, three-dimensional data collection, and subsequent data processing. This figure demonstrates that the banding pattern documented by Bridges (1935), as well as the bundles of chromatids seen in our unfixed samples, is clearly recognizable.

As well as requiring optimal chromosome structural preservation, it is equally important that the hybridization signal is a reproducible and accurate representation of the DNA. In situ hybridization has been performed using probes labeled with biotin or digoxigenin and subsequently detected using fluorescently labeled antibodies or streptavidin. Alternatively, to avoid secondary detection schemes, directly labeled, fluorescent probes have also been used. Although use of the directly labeled probes has reproducibly resulted in an approximately threefold decrease in the signal intensity, there is an equal decrease in the background staining. In a typical experiment, the in situ hybridization signal is visible in all nuclei in the acrylamide block, both opened nuclei and those with their nuclear envelopes still intact. The staining is equally strong on chromosomes at the bottom, close to the coverslip, and those at the top of the acrylamide block, suggesting that the acrylamide matrix does not interfere with the labeling process. Occasionally, within a sample there will be an area containing nuclei whose chromosomes look flattened and less well preserved; invariably these have a higher than average signal. For data collection, nuclei are chosen that have the best chromosome morphology by DAPI staining, regardless of the signal intensity. Finally, when we compare the substructural detail seen by DAPI staining with the in situ hybridization signal, we find that although not exact, there is an approximate overlap. Specifically, the signal does not spill out beyond the boundaries of the cylinder defined as the chromosome arm using DAPI staining, forming a tidy structure with discrete edges and cylindrical symmetry (see Fig. 7). Thus, we are confident that we have a system that allows accurate fine mapping of specific sequences on chromosomes that have retained their three-dimensional structural information.

We have used three-dimensional in situ hybridization, to investigate the characteristic substructure of individual bands. As with the DAPI staining pattern, we have found a punctate staining pattern in cross section, consistent with the idea that chromatids are bundled and also that the ar-

beled. *b* shows a gallery of individual DAPI-stained polytene chromosome bands that have been computationally isolated as described in Materials and Methods and volume rendered (Drebin et al., 1988). Each row shows a series of tilted views of a band from 0–50° by increments of 10° and can be viewed as a series of stereo pairs. Each band is cytologically identified in the left column using Bridges' revised map. Each band is scored for peripheral concentration of DNA (as described in Table I and text) to the right of each tilt series. The left side of panel *b* shows bands from the example of 3L shown above (Fig. 5 *a*). The right side of panel *b* shows the same bands that have been computationally dissected from another example of 3L. The view that corresponds to the image plane of optical sectioning is the left-most tilt; angle = 0°. Each band shows a dotted substructure with or without peripheral concentration of DNA. The scale bar represents 3 μm.

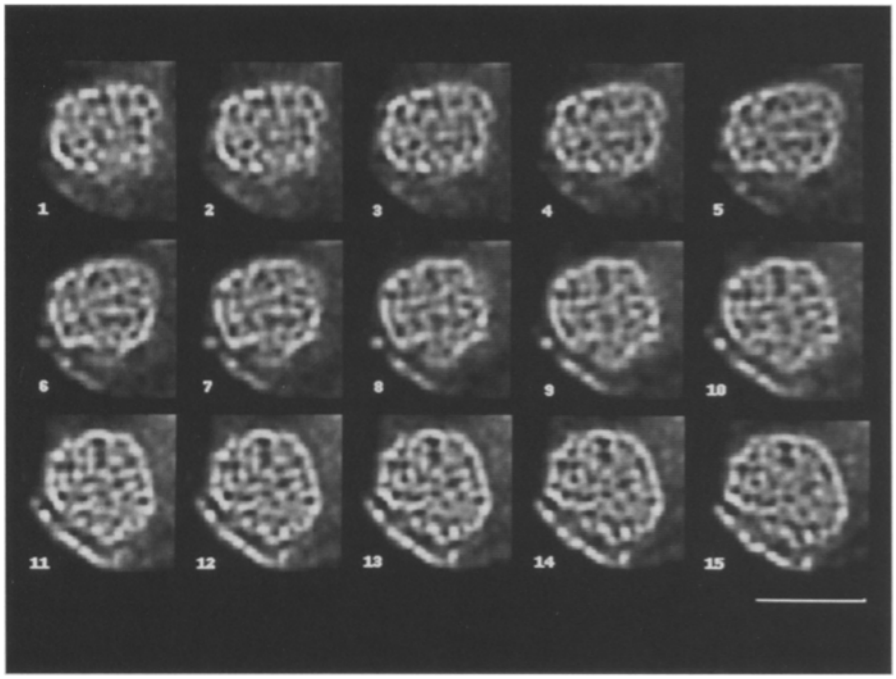

Figure 6. Optical, serial cross sections of a polytene chromosome arm are shown from an unfixed, urea-stripped nucleus that has been acrylamide embedded and stained with DAPI. The series begins with the upper leftmost image and images are numbered consecutively. Each view is 0.2-μm apart and clearly shows substructural features that can be traced through adjacent sections. The scale bar represents 3 μm.

rangement of those bundles varies in different bands. For example, for all 15 of the data sets collected using any of the *Notch* region probes (N_t, N_b, or N_i, described in Fig. 1), the in situ hybridization signal is always stronger around the periphery than in the center of the band, forming a toroid or sometimes a "horseshoe" shape. This characteristic shape is observed whether biotin, digoxigenin, or directly labeled probes are used. By contrast, the band containing the *white* gene (visualized by using w_t, a 34-kb probe mix, described in Fig. 1) has a reproducibly different distribution of chromatin (Fig. 7 *a*). Both the N_b and w_t probes used in Fig. 7 *a* include the coding region of the genes and can be seen, when compared to the DAPI staining, to hybridize to a band (3C7 and 3C2, respectively). Yet, while the N_b signal is concentrated at the periphery of the band, the w_t probe reveals a band that stains as brightly in the center as the periphery, implying that the peripheral concentration of an in situ signal is not merely an artifact arising from an inability of the probes or the fluorescent compounds to access the interior of the chromosome. We have also confirmed this difference between these two loci in less perturbed specimens. The 3C region was also imaged using isolated, unfixed nuclei that were treated to remove the nuclear envelopes, embedded in acrylamide and stained with DAPI. Computational dissection (as discussed in Materials and Methods) of the bands 3C2 and 3C7 (the *white* and *Notch* loci, respectively) are shown in Fig. 8. Again it can be seen that a greater portion of the DAPI staining structures are concentrated at the periphery of the band containing the *Notch* gene than the band containing the *white* gene, suggesting that the difference in the architecture of these two bands is not caused by variation in probes or the hybridization procedure. Thus, we believe that the differential staining seen at these two different loci indicates that the bundles of chromatids are organized differently at these two genes.

A Three-Dimensional Analysis of Polytene Chromosome Interbands

Although it is accepted that the DNA in the bands is more compacted than the DNA in the interbands, it is not clear how that translates in the polytene to changes in the path of individual chromatids or even bundles of chromatids. It is therefore of interest to compare the bands with their adjacent interbands. The very nature of interbands makes them difficult to study by fluorescence microscopy using DAPI staining because they stain so much less brightly (by a factor of 10–20) than the neighboring bands. However, it has been shown that RNA II is localized in the interbands of polytene chromosomes (Jamrich et al., 1977*b*, Krämer et al., 1980; Sass, 1982, Sass and Bautz, 1982). Thus, one method we have used to selectively highlight interbands is by immunofluorescence using anti-polymerase II antibodies. As a control for antibody accessibility, immunodetection sensitivity and specificity, we stained our three dimensional polytene chromosome preparations with a monoclonal antibody that recognizes all the histones. Images acquired with this histone antibody shows identical substructural and topological features to DAPI images (Fig. 4). Additionally, this control demonstrates that internal structures are accessible to IgG molecules. We have also compared fixed DAPI stained chromosomes, after immunostaining, with unfixed nuclei controls and find that the band morphology is not distorted (compare Figs. 4 and 9). Having established that our protocol is capable of yielding high resolution information by immunocytochemistry, we stained polytene chromosomes with anti-RNA polymerase II antibodies. In agreement with previous studies (Jamrich et al., 1977*a*; Krämer et al., 1980; Weeks et al., 1993), we find that RNA polymerase II is localized to interbands and puffs, and is not colocalized with the condensed chromatin of a band (Fig. 9). Our analysis has been done by inspection of stereo pairs as well as by com-

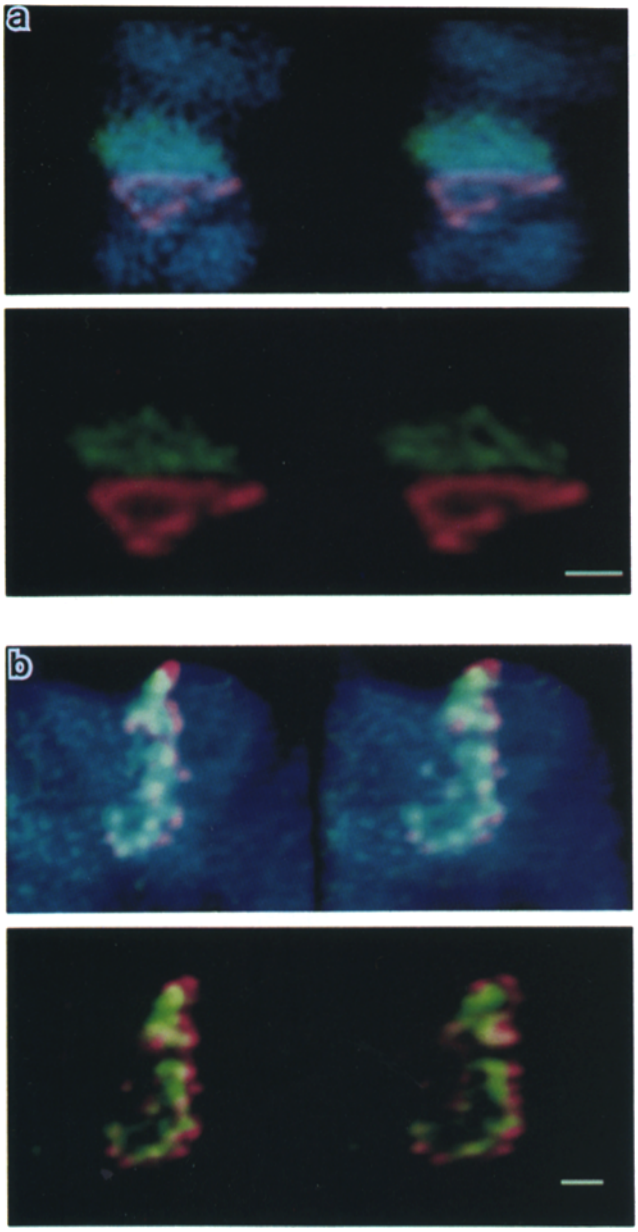

Figure 7. Stereo pairs are shown of two examples of double label in situ hybridization using probes from the 3C region. *a* compares the signals acquired using probes that encompass the coding regions for *white* (shown in *red*) and *Notch* (shown in *green*). These genes have been labeled using a biotin-labeled probe, w_t, and streptavidin fluorescein to show *white* and a digoxigenin-labeled probe, N_b, in conjunction with a rhodamine-labeled antibody to show *Notch*. *b* shows a comparison of band and interband signals from the *Notch* band, 3C7. A biotin-labeled probe, N_b, visualized using streptavidin fluorescein and a digoxigenin-labeled probe, N_i, visualized using a rhodamine-labeled antibody are hybridized to the 3C7 band (in *green*) and the 3C7/3C9-10 interband (in *red*), respectively. See text and Fig. 1 for description of the probes. In the top half of each panel signals are shown overlaid on the DAPI stained chromosome (in *blue*). The bottom half of each panel shows the hybridization signals without the DAPI signal. The telomere is down in *a* and to the right in *b*. Scale bars are 1 μm.

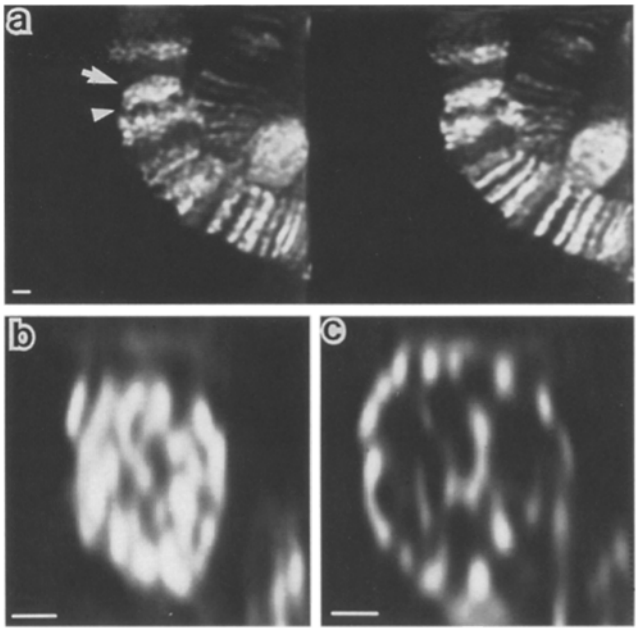

Figure 8. An unfixed, unhybridized polytene X chromosome has been DAPI stained and "computationally dissected." *a* is a stereo pair showing the 3C region, viewed in the same plane as it was optically sectioned. The band 3C2 (*arrow*) and the band 3C7 (*arrowhead*) have been computationally cut out and are shown in cross sections *b* and *c*, respectively. Scale bars 1 μm.

putational dissection of interbands and their immediate neighboring bands. As was observed with the DAPI staining or anti-histone labeling of bands, we find the anti-RNA polymerase II–labeled interbands are composed of substructural features as if the chromatids are bundled. When viewed in cross section, each interband is composed of dotted or ellipsoid substructures of variable intensities sized ~0.2–0.3 μm in diameter. The number of substructural components counted in an interband ranges between 18–38 (mean = 30 ± 5). This analysis includes 24 bands from six data sets from two different preparations. Fig. 9 shows an example of a polytene chromosome that has been double labeled with RNA polymerase II and DAPI. Data has been collected as longitudinal optical sections of the polytene chromosome arm, and then adjacent bands and interbands have been computationally dissected and displayed in cross section. Careful inspection of these neighboring bands and interbands reveals a structural relationship. There is a conservation of overall shape of the chromosome arm between a band and a neighboring interband and it is possible to find bundles of chromatids that appear to correspond between band and adjacent interband (*arrows*, Fig. 9 *c*).

Another approach we have taken to analyzing the relationship of bands and interbands is to use DNA in situ hybridization with band-specific and interband-specific probes. To label band and interband simultaneously, we have used Texas red to label the interband-specific probes and fluorescein to label the band-specific probes. An example of such a double label experiment is shown in Fig. 7 *b*. The band 3C7, corresponding to the *Notch* locus, was labeled by the N_b probe and the interband corresponding to the

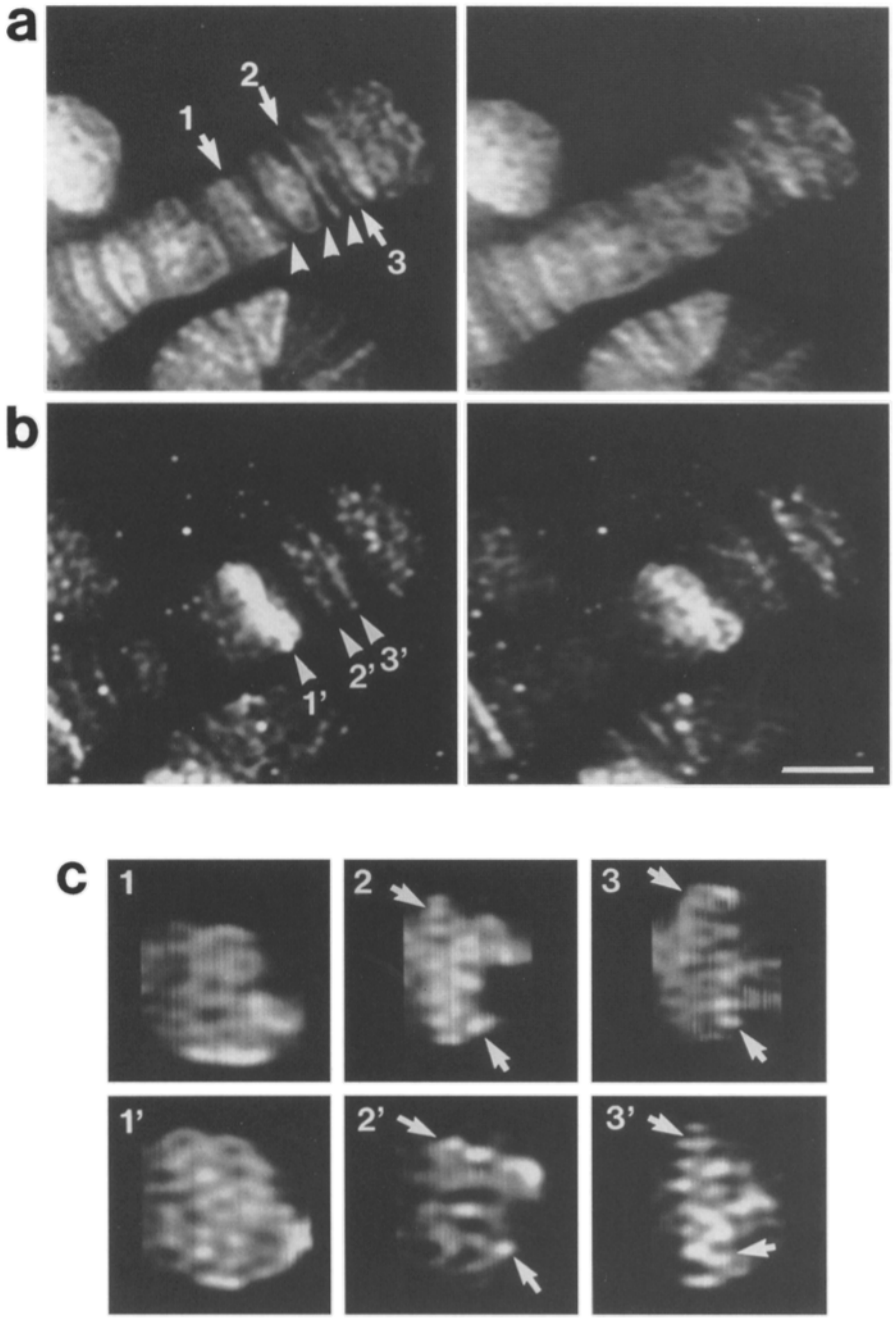

Figure 9. Immunolocalization of RNA polymerase II. Stereo pairs are shown of a tip of 2L that has been stained with DAPI (*a*) and stained with Texas red by indirect immunofluorescent detection of RNA polymerase II (*b*). The three bands that have been numbered are (reading from proximal to distal) 21E1-2 (*1*), 21C6 (*2*), and 21C4 (*3*). These bands (*arrows*) and their adjacent interbands (*arrowheads*) have been computationally dissected from the DAPI image and the Texas red image, respectively. Isolated, tilted views (20°) are shown of the bands (*top row* of *c*) and their neighboring interbands (*bottom row* of *c*). The general shape of the band is maintained in the adjacent interband and some substructural features can be followed band to interband (*arrows* in *c*). The scale bar represents 3 μm.

interval between bands 3C7 and 3C9-10 (sequences 3′ of the *Notch* gene) was labeled by the N_i probe (probes described in Materials and Methods and Fig. 1). A total of 0.6 kb separates the two mixes. These probes were chosen based on previous DNA in situ hybridization data from chromosome spreads (Rykowski et al., 1988). In Fig. 7 *b* it can be seen that the two sets of probes label adjacent but distinct regions with a very slight overlap. Furthermore, the DNA in the interband closely follows the structure of the DNA in the band. The peripheral localization of chromatin, characteristic of the band 3C7, clearly continues in the adjacent interband. Taken together with the observation from DAPI stained nuclei, it appears that the bundles of chromatids seen in the bands are also present in the interbands as though they form fibers that run longitudinally through the chromosome arm. Furthermore, whatever factors regulate the arrangement of bundles relative to one other, creating a band-specific architecture, are also in effect in the neighboring interband.

Alignment

As multiple labels are used in close proximity, it becomes necessary to consider how accurately the resulting data stacks are aligned. One possible source of misalignment may come from the use of an indirect detection (i.e., biotin-streptavidin or digoxigenin and an antibody) that may cause the signal to spread and be a less accurate represen-

tation of the location of the chromosomal DNA. This can be avoided by using directly labeled probes or antibodies. Another source of uncertainty comes from the expected small shifts resulting from wavelength dependent differences in magnification and translation. This phenomena is a fundamental property of optical components such as objective lenses and dichroic mirrors and is compounded by the conditions found when imaging biological specimens at substantial depths below the glass coverslip (Hiraoka et al., 1991). To quantify this effect we have collected data from in situ hybridization experiments using identical probes labeled with different fluorophores. The two resulting three-dimensional DNA images have been computationally aligned using a simplex method to correct for image shift and magnification differences (Swedlow, J., S. Parmelee, H. Itoi, J. Sedat, and D. Agard, manuscript in preparation). After alignment, the signals have the same general shape and cover the same area, however, they are not precisely identical. There are very small differences; substructural features are sometimes highlighted in one color or the other (data not shown). It is important to point out that by using multi-wavelength dichroic mirrors, the offset between the different images, before the simplex alignment, is never more than one pixel (0.074 microns) in X or Y or two pixels (0.4 microns) in Z. This offset has been confirmed using fiducial markers such as fluorescent beads (Rykowski et al., 1988) or an internal standard based on imaging the residual DAPI signal in the rhodamine channel. We therefore conclude that the similarities and differences seen between band and interband reflect the true structure of the chromosome rather than any optical aberration.

Discussion

A Methodology for the Alignment of Specific DNA Sequences to Three-Dimensional Chromosome Structures

From our experiments it is clear that there is a distinct organization for the chromatin that comprises the polytene bands and interbands. We find that in the cross sectional views of both bands and interbands, the chromatin is arranged in ~36 substructural features that have a diameter of 0.2–0.4 μm, in agreement with the idea that there is a bundling of chromatids. While some bands show an even distribution of chromatid bundles, a large portion of the bands, in many cases cytologically identified, have a distinct peripheral concentration of DNA. We have observed that this architecture may be a reproducible characteristic of a specific band. We also find a similarity in the arrangement of bundles of chromatids between neighboring bands as well as between neighboring bands and interbands as though the factors that govern the relationship of bundles of chromatids acts over a greater distance that the factors that control the boundaries of individual bands. Our approach is based on a novel method for preparing intact polytene chromosomes followed by a full three-dimensional reconstruction of the bands and interbands. This system allows us to use a combination of complementary methodologies. DAPI staining allows us to look at a global view of all bands in minimally perturbed, unfixed nuclei. One of the advantages of DAPI is that it is a nonintercalating dye that binds to the minor groove of DNA, thus perturbations of the DNA structure upon binding are minimized (Larsen et al., 1989). Although DAPI can show a preference for AT rich sequences, the staining patterns observed on polytene chromosomes with DAPI and antibodies to histones is nearly indistinguishable. We find that the structural features visualized by DAPI staining (the punctate pattern seen in cross sectional views of bands and the preponderance of bands with a brighter staining at the periphery) are also seen by immunostaining using monoclonal antibodies to histones (see Fig. 4).

We have further taken advantage of immunostaining as a method to acquire a three-dimensional understanding of interbands by imaging the location of RNA polymerase II. Strictly speaking this key transcriptional component may not exactly coincide with the DNA in the interband but is likely to be very close since interbands are active sites of transcription (Zhimulev et al., 1981*a*) and costaining of nuclei with DAPI shows no overlap of DAPI-bright bands and RNA polymerase II stained interbands (within 1–2 pixels). Finally, we have been able to perform DNA in situ hybridization on these opened, acrylamide-stabilized nuclei allowing, for the first time, the alignment of molecular DNA sequence information within the three-dimensional context of the polytene chromosome. This method of labeling band- or interband-specific structures also provides data consistent with the bundling of chromatids and confirms the heritability of band shapes as well as the continuity of chromatin organization between adjacent bands and interbands. We were initially concerned that the conditions necessary to perform in situ hybridization would alter chromosomes structures. However, we are convinced that this is not a problem for a number of reasons. In addition to the agreement between various methods of preparation discussed in this paper, the results from complementary experiments using the same buffers and denaturation conditions, indicate that chromosome structures are not disrupted. For instance, DNA in situ hybridization carried out on intact *Drosophila* embryos reveals chromosomal arrangements and dimensions and cytological staining patterns of prophase nuclei and metaphase figures that are indistinguishable from unhybridized controls (Hiraoka et al., 1993). Furthermore, the dimensions and overall appearance of in situ hybridized nuclear structures and metaphase figures are comparable to that seen by three dimensional in vivo image recordings (Dernburg, A., and J. Swedlow, University of California, San Francisco, personal communication). Experiments aimed at specifically perturbing the embedded chromosomes, such as treatment with high salt, formamide or heat, even on unfixed nuclei, result in well preserved morphology (data not shown) leading us to surmise that the acrylamide is acting as a strong support medium for chromosomal structures.

Any interpretation of three-dimensional studies using optical microscopy must consider the resolution limits in the Z axis. Three-dimensional optical transfer considerations dictate that the structures will be elongated and distorted along the Z axis (Agard et al., 1989). Our deconvolution methodologies act to improve resolution in all directions. Inspection of cross sections of the small substructural features indicates that the resolution of the Z di-

rection remains worse than in the X and Y directions by a factor of two or three. Comparisons of cross sections of bands displayed as X-Y planes and Y-Z planes show that the smearing in Z does not prohibit our quantifying the substructural features (compare Figs. 5, 6, 8, and 9). We therefore feel confident that the structures we observe are real and are not artifacts of sample preparation or imaging distortions.

Polytene Chromosome Substructural Organization

This study shows that there is a consistent 0.2–0.4 μm diameter chromosomal substructure making up the band. Objects of this dimension are close to the resolution limit of the light microscope. Thus, their actual size may be smaller. An average of 36 ± 7 substructural units are seen in the cross section of a band. Averages within one chromosome arm had a much smaller standard of deviation making it likely that the difference reflects small differences in degrees of polytenization or particular timing of bands with respect to the DNA replication. The number of substructural features found per band is consistent between three-dimensional images rotated to visualize cross sections and bands that were fortuitously imaged in cross section in the original data.

The relatively small number of substructural units per band suggests that each substructure must contain multiple chromatids. This bundling of chromatids has been previously observed in transmitted electron microscope studies (Ananiev and Barsky, 1985). Scanning electron microscopy provides evidence for a similar organization of polytene chromatin in *Chironomus* (Pelling and Allen, 1993). Pelling and Allen (1993) calculate the number of chromatids per bundle in *Chironomus* polytene chromosomes to be between 8 and 32. Given that we find 25–53 bundles per band and assuming that these chromosomes are composed of 1024 strands of DNA (2^{10} or ten rounds of DNA replication), we would calculate that there are ~20–40 chromatids per bundle.

Moreover, the intensity of substructural features is variable suggesting that there is a variability in the number of chromatids per bundle. It is possible that the grouping of chromatids in these bundles may change relative to the replication of DNA or transcriptional activity. The variability that we find as well as the observation that bundles merge and separate from each other along the chromosome length (see Fig. 6), suggests a fairly dynamic structure.

Band Specific Architecture

Previous two-dimensional data agrees with the concept of band specific architecture. Distinct band configurations, have been seen either by single sections or in squashed specimens by other investigators, appearing as dotted or solid bands (Bridges, 1935; Sass, 1980; Mott and Hill, 1986; Sorsa, 1988*c*). However, since the method of chromosome preparation has distorted structures and retains only a single plane of information, these observations are difficult to interpret. Another characteristic of bands that has long been documented is Bridges doublets. The significance of this distinction remains unresolved: whether they are one band, or two bands or an artifact of fixation. It has been suggested that the doublet appearance of bands may be due to vacuoles that are induced by acid fixation (Berendes, 1970; Lefevre, 1976; Saura and Sorsa, 1979; Zhimulev et al., 1981*b*). Mott and Hill (1986) further suggest that this may be an enlargement of much smaller vacuoles that normally exist in some bands. Since we see evidence that the peripheral concentration of DNA may be a reproducible characteristic of specific bands, we have attempted to correlate the occurrence of bands that have a greater degree of peripheral concentration with the classification of those bands as doublets. Our results (Fig. 5, Table I) do not support the idea that band architecture alone is the difference between the singlet and doublet bands seen in acid-fixed, squashed specimens.

By using an isolation method that allows the chromosomes to be prepared without squashing, stretching and for much of the data collected here, without fixation, we have a minimally perturbed system for analysis of the full three-dimensional structure. Computational isolation of bands from unfixed, DAPI stained chromosomes show that some bands display a reproducible architecture. However, we have only two or three examples of each band using this methodology. A more complete sampling done at the *Notch* locus by in situ hybridization reveals a consistent shape in all 15 examples. Taken together, these results provide unambiguous data to support the hypothesis that specific bands have a characteristic architecture.

When the *Notch* locus (band 3C7) and the *white* locus (3C2) are isolated either by in situ hybridization with sequences specific to the coding region of the gene, or by computational dissection of DAPI stained, unfixed chromosomes, each band consistently shows a characteristic arrangement of substructural features. While the *Notch* locus always shows a greater concentration of DNA in the periphery of the band, the *white* locus consistently has a more uniform distribution of chromatid bundles. No exceptions were observed after looking at many examples in multiple distinct preparations. It appears that *Notch* is one of a limited number of bands that have their DNA concentrated as a small shell of approximately the band thickness at the band periphery, forming a toroid. This class of bands represents one extreme of a continuum of band architectures with varying degrees of peripheral DNA concentration. Occasionally the band 3C7 looks like a toroid with one end opened resembling a horseshoe. Evidence of a horseshoe shaped variation of band structure has previously been suggested to reflect an opening of the closed toroid configuration, possibly at the juncture point of the two homologs (Mortin and Sedat, 1982).

Because of this apparent conservation of band architecture, we suggest that there may be some functional significance to the shape of the band. The variation of band architecture between the extremes may occur for a given band depending on developmental state (Berendes, 1970), transcriptional activity (Ananiev and Barsky, 1978; Semeshin et al., 1979), or distinct phases of the DNA replication cycle (Crouse and Keyl, 1968; Arcos-Terán, 1972). We do not have a ready explanation for the peripheral concentration of DNA in a band. Potentially the interiors could serve as specific sites for DNA replication, or low level transcription, or places for sequestering, transporting or storing proteins involved in these processes. This is supported by the observation that ribonucleoprotein particles

are found in the interior of some bands (Mott and Hill, 1986). It is possible that rigorously untranscribed bands revert to a baseline architecture. Because neither *Notch* nor *white* have been identified as transcriptionally active genes in the salivary glands, the differences between *Notch* and *white* band architecture are probably not simply a difference in transcriptional states of the genes. It is possible, in addition, to have different degrees of DNA replication complicating the structure. Since all the nuclei from the salivary gland are used in the nuclear isolation procedure, our samples include chromosomes of varying extents of polytenization (2–4-fold differences). Thus the reproducibility of our results is an indication that the specific band architecture is stable despite the variable degree of replication. However, it is possible that at some earlier stage of polytenization band differences are not distinguished. When we have broadened our base of study to include genes studied at a variety of different stages of gene activity and levels of polyteny, we should be able to learn how changes in band architecture relate to various states of transcription or DNA replication.

Correlation of Substructural Features from Band to Interband and from Band to Band

Although we have focused on the substructural features visible in specific bands, we are also interested in the correlation of these features with the rest of the polytene chromosome. It is possible to trace a bundle of chromatids through serial cross sections in DAPI stained images (Fig. 6). Likewise, computational cross sections of adjacent bands, such as in Fig. 5, give the impression of bundles that are traceable across multiple bands. This is in agreement with scanning electron micrographs of *Chironomus* polytenes chromosomes (Pelling and Allen, 1993). We have also investigated the bundles of chromatids seen in interbands and observe approximately the same dimensions and number as seen in the band. Comparison of band-specific and interband-specific probes from the *Notch* region by in situ hybridization as well as comparison of DAPI stained bands with neighboring interbands by immunofluorescence using RNA polymerase II both reveal that the three-dimensional shape and substructure of the interband appears to parallel the adjacent band, reflecting, we suggest, a similar organization. This indicates a common long-range organization of chromatin spanning both noncoding and coding regions, effectively packing these different, but related DNA elements into a single structural domain. We suggest that bundles of chromatids are longitudinal features of the polytene chromosome arm, displaying continuity from band to interband and into an adjacent band. We find that changes in the arrangement of these substructural features relative to each other is slow, extending over several bands and suggesting that a chromatid follows a relatively straight path through the chromosome arm. Recent direct experiments, using fluorescent deoxynucleoside triphosphates to pulse label embryos, reveal that the diploid complement of DNA in these polytene chromosomes does follow a relatively straight path (Itoi, H., S. Parmelee, D. Agard, and J. Sedat, manuscript in preparation). This is in agreement with results of earlier experiments by Beermann (Beermann and Pelling, 1965).

The Cylindrical Symmetry of Polytenes

In a polytene chromosome, there must be a mechanism that maintains the alignment of sister chromatids. Any model for these mechanisms must take into account the chromosome's cylindrical shape. We suggest that there is a bundling of chromatids in both the bands and the interbands such that ~20–40 chromatids are arranged in close proximity to each other. It is not clear whether this bundling of chromatids is a result of forces that push unit chromatids together or ones that push chromatids apart, or some combination of the two. The variation in band architecture implies that these forces are not the same in all bands. It is not obvious what limits the size of the substructural features (i.e., the number of chromatids per bundle) nor what determines the position of bundles relative to one another. It is of interest that the chromosome maintains a circular cylindrical shape, whether there are one or two homologs present. In fact, we see no evidence that there is any discontinuity within the polytene bands that make it possible to distinguish the two homologs. Yet, the fact that there are conditions that lead to a separation of homologs (e.g., the fixation conditions used by Bridges for squashes) as well as our finding of the ordered separation of homologs at sites of inversion forks indicate that chromatids from each homolog do not mix. One of the more intriguing questions about polytene chromosomes concerns the mechanisms that form and maintain cylindrical symmetry for the polytene chromosome band. What mechanisms coordinate the chromatin bundles into a distinct architecture like the toroid in the *Notch* case? It is likely that whatever mechanism determines the shape of specific bands is also influenced by the mechanisms involved in maintaining the cylindrical shape of the chromosome arms. These structures may be the result of interactions that are also at work in all interphase nuclei or they may be polytene specific.

Future Directions

This study represents a global view of the three-dimensional polytene chromosome band/interband structure. This top down approach has allowed us to make statements about band structures and overall polytene chromosome organization. It is now necessary to link our knowledge of the polytene chromosome band and interband structure with function. An ideal approach would be to use three-dimensional imaging of live salivary gland polytene chromosomes within intact nuclei in whole glands. Recently published reports emphasize the usefulness of in vivo labeling to monitor specific components of nuclear structure (Hiraoka et al., 1989; Swedlow et al., 1993). We anticipate using in vivo labeling schemes for specific three-dimensional bands and interbands. This should allow us to look for time-dependent structural changes during transcription and DNA replication. Structural studies also need to be extended to the three-dimensional EM level. Recent progress with automated tomographic schemes demonstrates a resolution of ~5 nm (Koster et al., 1993). This should allow us to better define the smaller substructures within bands and interbands in a true three-dimensional context. We believe that by focusing on preservation of structure at all stages of the experiments, we can

acquire data that is representative of the in vivo structures without sacrificing the additional information gained by working with the three-dimensional data.

We thank Susan Younger-Shepherd for providing the FM7 strain. We thank Dr. Hank Bass, Dr. Kelly Dawe, Dr. Jason Swedlow, Jennifer Fung, and Wallace Marshall for critical reading of the manuscript.

This work was supported by grants from the National Institutes of Health to J. W. Sedat (GM-25101) and D. A. Agard (GM-31627). J. W. Sedat and D. A. Agard are Howard Hughes Investigators.

Received for publication 5 August 1994 and in revised form 23 May 1995.

References

Agard, D. A., Y. Hiraoka, P. Shaw, and J. W. Sedat. 1989. Fluorescence microscopy in three dimensions. *Methods Cell Biol.* 30:353–377.

Ananiev, E. V., and V. E. Barsky. 1978. Localization of RNA synthesis sites in the 1B-3C region of the *Drosophila melanogaster* X chromosomes. *Chromosoma.* 65:359–371.

Ananiev, E. V., and V. E. Barsky. 1985. Elementary structures in polytene chromosomes of *Drosophila melanogaster. Chromosoma.* 93:104–112.

Arcos-Terán, L. 1972. DNS-Replikation und die Natur der spät replizierenden Orte im X-Chromosom von *Drosophila melanogaster. Chromosoma (Berl.).* 37:233–296.

Ashburner, M. 1967. Patterns of puffing activity in the salivary gland chromosomes of *Drosophila* I. Autosomal puffing patterns in a laboratory stock of *Drosophila melanogaster. Chromosoma.* 21:398–428.

Ashburner, M. 1972. Puffing patterns in *Drosophila melanogaster* and related species. *In* Developmental Studies on Giant Chromosomes. Vol. 4. W. Beermann, editor. Springer-Verlag, Berlin, Heidelberg, New York. 101–147.

Beermann, W. 1972. Chromomeres and genes. *In* Developmental Studies on Giant Chromosomes. Vol. 4. W. Beermann, editor. Springer-Verlag, Berlin, Heidelberg, New York. 1–33.

Beermann, W., and C. Pelling. 1965. H^3-Thymidin-Markierung einzelner Chromatinden in Riesenchromosomen. *Chromosoma.* 16:1–21.

Belmont, A. S., M. B. Braunfeld, J. W. Sedat, and D. A. Agard. 1989. Large-scale chromatin structural domains within mitotic and interphase chromosomes in vivo and in vitro. *Chromosoma.* 98:129–143.

Berendes, H. D. 1965. Salivary gland function and chromosomal puffing patterns in *Drosophila hydei. Chromosoma (Berl.).* 17:35–77.

Berendes, H. D. 1970. Polytene chromosome structure at submicroscopic level. I. A map of region X,1-4E of *Drosophila melanogaster. Chromosoma (Berl.).* 29:118–130.

Bridges, C. B. 1935. Salivary chromosome maps with a key to the banding of the chromosomes of *Drosophila melanogaster. J. Heredity.* 26:60–64.

Bridges, P. N. 1942. A new map of the salivary 2L-chromosome of *Drosophila melanogaster. J. Heredity.* 33:403–408.

Burgoyne, L. A., M. Anwar Waqar, and M. R. Atkinson. 1970. Calcium-dependent priming of DNA synthesis in isolated rat liver nuclei. *Biochem. Biophys. Res. Commun.* 39:254–259.

Chen, C. N., T. Malone, S. K. Beckendorf, and R. L. Davis. 1987. At least two genes reside within a large intron of the *dunce* gene of *Drosophila. Nature (Lond.).* 329:721–724.

Chen, H., J. W. Sedat, and D. A. Agard. 1989. Manipulation, display, and analysis of three-dimensional biological images. *In* Handbook of Biological Confocal Microscopy. J. B. Pawley, edtior. Plenum Press, New York and London. 141–150.

Crouse, H. V., and H. G. Keyl. 1968. Extra replications in the "DNA-puffs" of *Sciara coprophila. Chromosoma (Berl.).* 25:357–364.

Drebin, R. A., L. Carpenter, and P. Hanrahan. 1988. Volume rendering. *Computer Graphics.* 22:51–58.

DuPraw, E. J., and M. M. Rae. 1966. Polytene chromosome structure in relation to the "folded fibre" concept. *Nature (Lond.).* 212:598–600.

Eveleth, D. D., and J. L. Marsh. 1987. Overlapping transcription units in Drosophila sequence and structure of the Cs gene. *Mol. & Gen. Genet.* 209:290–298.

Giloh, H., and J. W. Sedat. 1982. Fluorescence microscopy: reduced photobleaching of rhodamine and fluorescein protein conjugates by *n*-propyl gallate. *Science (Wash. DC).* 217:1252–1255.

Grant, D. H., J. N. Miller, and D. Thorburn Burrs. 1973. The fluorescence properties of polyacrylamide gels. *J. Chromatography.* 79:267–273.

Henikoff, S., M. A. Keene, K. Fechtel, and J. W. Fristrom. 1986. Gene within a gene: nested *Drosophila* genes encode unrelated proteins on opposite DNA strands. *Cell.* 44:33–42.

Hill, R. J., and F. Watt. 1977. "Native" salivary chromosomes of *Drosophila melanogaster. Cold Spring Harbor Symp. Quant. Biol.* 42:859–865.

Hill, R. J., and S. Whytock. 1993. Cytological structure of the native polytene salivary gland nucleus of *Drosophila melanogaster*: a microsurgical analysis. *Chromosoma.* 102:446–456.

Hiraoka, Y., A. F. Dernburg, S. J. Parmelee, M. C. Rykowski, D. A. Agard, and J. W. Sedat. 1993. The onset of homologous chromosomal pairing during *Drosophila melanogaster* embryogenesis. *J. Cell Biol.* 120:591–600.

Hiraoka, Y., J. S. Mindanao, J. R. Swedlow, J. W. Sedat, and D. A. Agard. 1989. Focal points for chromosome condensation and decondensation revealed by three-dimensional *in vivo* time-lapse microscopy. *Nature (Lond.).* 342:293–296.

Hiraoka, Y., J. W. Sedat, and D. A. Agard. 1990. Determination of three-dimensional imaging properties of a light microscope system, partial confocal behavior in epifluorescence microscope. *Biophys. J.* 57:325–333.

Hiraoka, Y., J. R. Swedlow, M. R. Paddy, D. A. Agard, and J. W. Sedat. 1991. Three-dimensional multiple-wavelength fluorescence microscopy for the structural analysis of biological phenomena. *Semin. Cell Biol.* 2:153–165.

Hochman, B. 1971. Analysis of chromosome 4 in *Drosophila melanogaster.* II. Ethyl methanesulfonate induced lethals. *Genetics.* 67:235–252.

Jamrich, M., A. L. Greenleaf, and E. K. F. Bautz. 1977*a*. Localization of RNA polymerase in polytene chromosomes of *Drosophila melanogaster. Proc. Natl. Acad. Sci. USA.* 74:2079–2083.

Jamrich, M., A. L. Greenleaf, F. A. Bautz, and E. K. Bautz. 1977*b*. Functional organization of polytene chromosome. *Cold Spring Harbor Symp. Quant. Biol.* 42:389–396.

Johnson, G. D., R. S. Davidson, K. C. McNamee, G. Russell, D. Goodwin, and E. J. Holborow. 1982. Fading of immunofluorescence during microscopy: a study of the phenomenon and its remedy. *J. Immunol. Methods.* 55:231–242.

Kam, Z., M. O. Jones, H. Chen, D. A. Agard, and J. W. Sedat. 1993. Design and construction of an optimal illumination system for quantitative wide-field multi-dimensional microscopy. *Bioimaging.* 1:71–81.

Keppy, D. O., and W. J. Welshons. 1980. The synthesis of compound bands in *Drosophila melanogaster* salivary glands chromosomes. *Chromosoma.* 76: 191–200.

Kidd, S., T. J. Lockett, and M. W. Young. 1983. The *Notch* locus of *Drosophila melanogaster. Cell.* 34:421–433.

Koster, A. J., M. B. Braunfeld, J. C. A. Fung, C. K. Abbey, K. F. Han, W. Liu, H. Chen, and J. W. Sedat. 1993. Towards automatic three-dimensional imaging of large biological structures using intermediate voltage electron microscopy. *Microscopic Society of America.* 23:176–188.

Krämer, A., R. Haars, R. Kabisch, H. Will, F. A. Bautz, and E. K. F. Bautz. 1980. Monoclonal antibodies directed against RNA polymerase II of D. melanogaster. *Mol. & Gen. Genet.* 180:193–199.

Kuo, C.-H., H. Giloh, A. B. Blumenthal, and J. W. Sedat. 1982. A library of monoclonal antibodies to nuclear proteins from *Drosophila melanogaster* embryos. *Exp. Cell Res.* 142:141–154.

Larsen, T. A., D. S. Goodsell, D. Cascio, K. Grzeskowiak, and R. E. Dickerson 1989. The structure of DAPI bound to DNA. *J. Biomol. Struct. & Dyn.* 7: 477–491.

Lefevre, G., Jr. 1974. The relationship between genes and polytene chromosome bands. *Ann. Rev. Genet.* 8:51–62.

Lefevre, G. 1976. A photographic representation and interpretation of the polytene chromosomes of *Drosophila melanogaster* salivary glands. *In* The Genetics and Biology of *Drosophila.* Vol. 1a. M. Ashburner and E. Novitski, editors. Academic Press, New York. 31–66.

Levis, R., P. M. Bingham, and G. Rubin. 1982. Physical map of the *white* locus of *Drosophila melanogaster. Proc. Natl. Acad. Sci. USA.* 79:564–568.

Mortin, L. I., and J. W. Sedat. 1982. Structure of *Drosophila* polytene chromosomes, evidence for a toroidal organization of the bands. *J. Cell Sci.* 57:73–113.

Mott, M. R., and R. J. Hill. 1986. The ultrastructural morphology of native salivary gland chromosomes of *Drosophila melanogaster*: the band-interband question. *Chromosoma (Berl.).* 94:403–411.

Paul, J. S., and G. M. Mateyko. 1970. Quantitative interference microscopy of polytene chromosomes. II. Cytochemical studies via ultramicrospectrophotometry. *Exp. Cell Res.* 59:237.

Pelling, C., and T. D. Allen. 1993. Scanning electron microscopy of polytene chromosomes (I). *Chromosome Research.* 1:221–237.

Rykowski, M. C., S. J. Parmelee, D. A. Agard, and J. W. Sedat. 1988. Precise determination of the molecular limits of a polytene chromosome band: regulatory sequences for the *Notch* gene are in the interband. *Cell.* 54:461–472.

Sass, H. 1980. Hierarchy of fibrillar organization levels in the polytene interphase chromosomes of *Chironomus. J. Cell Sci.* 45:269–293.

Sass, H. 1982. RNA polymerase B in polytene chromosomes: immunofluorescent and autoradiographic analysis during stimulated and repressed RNA synthesis. *Cell.* 28:269–278.

Sass, H., and E. K. F. Bautz. 1982. Interbands of polytene chromosomes: binding sites and start points for RNA polymerase B(II). *Chromosoma.* 86:77–93.

Saura, A. O., and V. Sorsa. 1979. Electron microscopic analysis of the banding pattern in the salivary gland chromosomes of *Drosophila melanogaster* Divisions 21 and 22 of 2L. *Hereditas.* 90:39–49.

Sedat, J., and L. Manuelidis. 1977. A direct approach to the structure of eukaryotic chromosomes. *Cold Spring Harbor Symp. Quant. Biol.* 42:331–350.

Semeshin, V. F., E. S. Belyaeva, I. F. Zhimulev, J. T. Lis, G. Richards, and M. Bourouis. 1986. Electron microscopic analysis of Drosophila polytene chromosomes IV. Mapping of morphological structures appearing as a result of transformatin of DNA sequences into chromosomes. *Chromosoma.* 93:461–468.

Semeshin, V. F., S. A. Demakov, M. Perez Alonso, E. S. Belyaeva, J. J. Bonner, and I. F. Zhimulev. 1989. Electron microscopical analysis of *Drosophila* polytene chromosomes. V. Characteristics of structures formed by trans-

posed DNA segments of mobile elements. *Chromosoma.* 97:396–412.
Semeshin, V. F., I. F. Zhimulev, and E. S. Belyaeva. 1979. Electron microscope autoradiographic study on transcriptional activity of *Drosophila melanogaster* polytene chromosomes. *Chromosoma.* 73:163–177.
Shaw, P. J., D. A. Agard, Y. Hiraoka, and J. W. Sedat. 1989. Tilted view reconstruction in optical microscopy. Three-dimensional reconstruction of *Drosophila melanogaster* embryo nuclei. *Biophys. J.* 55:101–110.
Smith, A. V., and T. L. Orr-Weaver. 1991. The regulation of the cell cycle during *Drosophila* embryogenesis: the transition of polyteny. *Development.* 112: 997–1008.
Sorsa, V. 1983. Toroidal bands in polytene chromosomes of *Drosophila. J. Cell Sci.* 64:255–264.
Sorsa, V. 1988*a*. Chromosomal localization of genes in *Drosophila melanogaster* A. The X chromosome. *In* Chromosome Maps of *Drosophila.* Vol. 1. CRC Press, Inc., Boca Raton, FL. 110–122.
Sorsa, V. 1988*b*. Functional models of polytene chromosomes. *In* Chromosome Maps of *Drosophila.* Vol. 1. CRC Press, Inc., Boca Raton, FL. 129–135.
Sorsa, V. 1988*c*. Ultrastructure of polytene chromosomes. *In* Chromosome Maps of *Drosophila.* Vol. 1. CRC Press, Inc., Boca Raton, FL. 55–90.
Spierer, A., and P. Spierer. 1984. Similar level of polyteny in bands and interbands of *Drosophila* giant chromosomes. *Nature (Lond.).* 307:176–178.
Spierer, P., and A. Spierer. 1983. Molecular mapping of genetic and chromomeric units in *Drosophila melanogaster. J. Mol. Biol.* 168:35–50.
Swedlow, J. R., J. W. Sedat, and D. A. Agard. 1993. Multiple chromosomal populations of topoisomerase II detected in vivo by time-lapse, three dimensional wide-field microscopy. *Cell.* 73:97–108.
Weeks, J. R., S. E. Hardin, J. Shen, J. M. Lee, and A. L. Greenleaf. 1993. Locus-specific variation in phosphorylation state of RNA polymerase II in vivo: correlations with gene activity and transcript processing. *Genes Dev.* 7:2329–2344.
Young, M. W., and B. H. Judd. 1978. Nonessential sequences, genes, and the polytene chromosome bands of *Drosophila melanogaster. Genetics.* 88:723–742.
Zhimulev, I. F., and E. S. Belyaeva. 1975. ^{3}H-Uridine labeling patterns in the *Drosophila melanogaster* salivary gland chromosomes X, 2R and 3L. *Chromosoma (Berl.).* 49:219–231.
Zhimulev, I. F., and E. S. Belyaeva. 1991. Chromomeric organization of polytene chromosomes. *Genetica.* 85:65–72.
Zhimulev, I. F., E. S. Belyaeva, and V. F. Semeshin. 1981*a*. Informational content of polytene chromosome bands and puffs. *CRC Crit. Rev. Biochem.* 11: 303–340.
Zhimulev, I. F., G. V. Polholkova, A. V. Bgatov, V. F. Semeshin, and E. S. Belyaeva. 1981*b*. Fine cytogenetical analysis of the band 10A1-2 and the adjoining regions in the *Drosophila melanogaster* X chromosome. II. Genetic analysis. *Chromosoma.* 82:25–40.